

RESEARCH ARTICLE

10.1002/2017JD027079

Special Section:

Atmospheric Gravity Wave Science in the Polar Regions and First Results from ANGWIN

Key Points:

- Upward propagating gravity wavefield in lower stratosphere dominated by low-frequency, short vertical wavelength waves
- Downward propagating wavefield in lower stratosphere contains waves with a wider range of wavelengths and many at higher frequencies
- In wintertime the downward propagating waves contribute as much as upward propagating waves to the energy density and momentum fluxes

Correspondence to:

T. Moffat-Griffin,
tmof@bas.ac.uk

Citation:

Moffat-Griffin, T., and S. R. Colwell (2017), The characteristics of the lower stratospheric gravity wavefield above Halley (75°S, 26°W), Antarctica, from radiosonde observations, *J. Geophys. Res. Atmos.*, 122, 8998–9010, doi:10.1002/2017JD027079.

Received 4 MAY 2017

Accepted 25 JUL 2017

Accepted article online 11 AUG 2017

Published online 3 SEP 2017

© 2017 Crown copyright. This article is published with the permission of the Controller of HMSO and the Queen's Printer for Scotland.

The characteristics of the lower stratospheric gravity wavefield above Halley (75°S, 26°W), Antarctica, from radiosonde observations

T. Moffat-Griffin¹  and S. R. Colwell¹¹British Antarctic Survey, Cambridge, UK

Abstract Daily radiosonde observations between 2003 and 2013 from Halley research station, Antarctica (75°S, 26°W), are used to determine climatologies of gravity wave properties in the lower stratosphere (between 15 km and 22 km altitude). Individual waves are extracted from the radiosonde profile using wavelet analysis and separated into upward and downward propagating waves. An increase in the percentage of downward propagating waves (~30% of the waves) is seen during the winter months. For the upward and downward propagating waves, their horizontal and vertical wavelength, intrinsic frequency, energy density, pseudomomentum flux, and direction of propagation are determined. The upward propagating wavefield is found to be dominated by waves with short vertical wavelength (~1 km) and low intrinsic frequency ($\omega \sim f$). The downward propagating wavefield is composed of a wider distribution of vertical wavelength waves and has a larger proportion of higher-frequency waves present. The upward propagating waves show an increase in total energy density in autumn and spring; the larger increase occurs during spring (up to 1.7 J kg⁻¹ in September). The downward propagating waves increase in total energy density occurs during wintertime (up to 0.7 J kg⁻¹ in June). During winter the contributions of the upward and downward propagating waves to the total energy density and pseudomomentum flux are almost equal. This paper details the first study of individual gravity wave properties combined into upward and downward propagating wave climatologies in the lower stratosphere above Halley.

1. Introduction

Gravity waves play an important role in the driving of the middle atmosphere circulation [Fritts and Alexander, 2003]. These waves can be generated by a variety of mechanisms such as wind flow over mountains, storms, geostrophic adjustment, and the polar vortex. The typical short spatial scales of gravity waves are such that they have to be represented in global numerical models by parameterizations. Although there have been recent improvements in these parameterizations [Alexander et al., 2010; Garcia et al., 2017], there are still issues in some models where the Antarctic middle atmosphere temperatures are too cold (the “cold pole” problem) and the timing of the Antarctic polar vortex breakup being late [Garcia et al., 2017; McLandress and Scinocca, 2005]. These problems have been attributed to “missing” gravity waves in this region that are not represented by the models. The parameterizations can be refined by constraining them with further observations of gravity wave activity, thus improving the results from global numerical models.

Many observational stratospheric gravity wave studies over Antarctica have taken place using a range of instruments including: satellites [Alexander et al., 2009; Gong et al., 2012; Hindley et al., 2015; Wang and Alexander, 2010; Wu and Jiang, 2002], superpressure balloons [Hertzog et al., 2008, 2007], lidars [Yamashita et al., 2009], and radiosondes [Guest et al., 2000; Moffat-Griffin et al., 2011, 2013; Murphy et al., 2014; Pfenninger et al., 1999; Yoshiki and Sato, 2000; Yoshiki et al., 2004; Zink and Vincent, 2001a]. Each of these instruments can only observe part of the gravity wave spectrum; this is known as an “observational filter” [Alexander, 1998]. For example, radiosonde data sets are biased toward gravity waves with short vertical wavelengths. Satellites, however, have a range of viewing geometries which means that each one observes slightly different parts of the gravity wave spectrum. Typically, they can observe the longer vertical wavelengths (6 km and above), although some (e.g., COSMIC and HIRDLS) can detect vertical wavelengths down to ~3 km [Alexander et al., 2010; Wright et al., 2016]. In order to fully quantify the whole gravity wavefield measurements from different instruments need to be combined.

Radiosondes are an important data source to complete the whole picture of the gravity wavefield because of their ability to detect those gravity waves with very short vertical wavelengths.

Radiosondes are launched attached to a weather balloon which rises rapidly until it bursts (typically in the lower stratosphere). These data provide altitude profiles of parameters such as wind speed, wind direction, and temperature from the surface to the lower stratosphere.

The use of radiosondes to observe gravity waves in the troposphere and stratosphere is a well-established technique, and with the increase in use of high temporal resolution radiosondes since the late 1990s more detailed information about gravity waves have been able to be determined, with individual waves being identified in a given profile and their properties calculated. Radiosonde profiles are not vertical due their drift with horizontal winds; however, it can be assumed to have sampled the gravity wavefield without distortion when the rate of ascent of the radiosonde is fast enough compared to wave scales and wave frequency and the horizontal drift of the radiosonde is small (i.e., horizontal winds below $\sim 50 \text{ ms}^{-1}$) [Gardner and Gardner, 1993; Vincent *et al.*, 1997].

Over Antarctica there have been several climatological studies of gravity wave activity using radiosonde data, with some features being common to most sites: a large increase in the percentage of downward propagating waves in the wintertime (increasing to 60% of the wavefield at some locations [Moffat-Griffin *et al.*, 2011]) and an increase in energy density during the springtime. The generation of gravity waves observed in these studies have been attributed a range of sources, e.g., mountain wave activity, regions of cyclogenesis, the polar vortex, and regions of geostrophic adjustment in the stratosphere.

Studies have suggested that downward propagating waves are prevalent during the wintertime stratosphere, so their contribution to the stratospheric wavefield needs to be examined.

It is important to understand not just the local climatology at a given location but also the continent-wide variations [Moffat-Griffin *et al.*, 2016] if our understanding of the whole gravity wavefield and its variation are to be improved. Due to the nature of Antarctica, the research stations can be located great distances apart. In the current literature there has been no detailed study of gravity wave activity in the lower stratosphere using radiosondes in the 60°W–40°E longitude sector of Antarctica. A study of data from Halley station (75°35'S, 26°39'W) will start to fill in this "gap" in coverage.

Halley station is an Antarctic base run year-round by the British Antarctic Survey and is located on the Brunt Ice Shelf (Figure 1). The local topography is very flat with no mountains in the locality. Halley is located ~ 20 km from the edge of the permanent ice shelf and open ocean, although the presence of sea ice in the winter months extends this distance. Halley's location is such that it remains inside the stratospheric polar vortex for most of the winter months [Espy *et al.*, 2006].

Radiosonde observations from both Halley V and Halley VI stations, whose locations are separated by ~ 10 km, are used in this paper. Halley V was decommissioned in 2012, and all radiosonde launches from this time onward were from Halley VI. As the distance between the two sites is small compared to the vertical range of the radiosondes, it can be assumed that there will be no significant differences in the wavefield above the two sites.

This paper provides the first detailed study of the properties of individual gravity waves observed in radiosonde data in the lower stratosphere above Halley station, Antarctica (75°S, 26°W), that are combined into upward and downward propagating wave climatologies.

2. Data and Analysis

High-resolution radiosondes have been launched daily at 11 UT from Halley since 2000. Vertical profiles of pressure, temperature, humidity, dew point, wind speed, and wind direction are returned at 2 s intervals. The radiosondes reach altitudes ranging between 20 km and 30 km (during the winter months the burst height is much lower than in summer due to the difference in mean air temperature—lower temperatures reduce the elasticity of the balloon). The Vaisala RS80 radiosonde was used at Halley until 2005; after this date the system used is a Vaisala RS92 radiosonde [Vaisala, 2013]. Studies comparing the two types of radiosonde have shown that there is a very small difference in the daytime temperatures recorded (~ 0.7 K at 10 hPa) [Smout *et al.*, 2005; Steinbrecht *et al.*, 2008]. This difference will not bias the results in this paper as the gravity waves will be identified using the relative variations in the data not the absolute values.

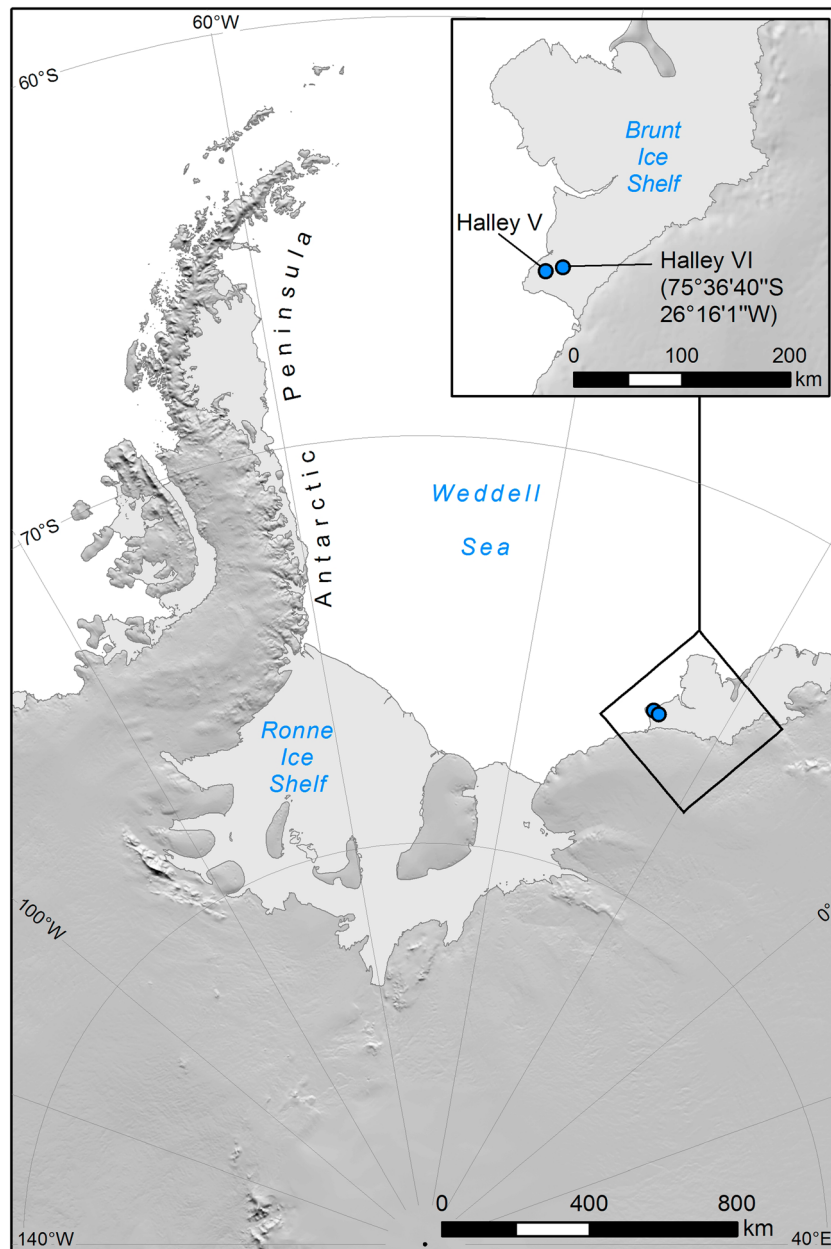


Figure 1. The location of Halley stations V and VI, Antarctica.

For the purposes of this study only radiosondes that reach 22 km and above are used. This is to ensure that a sufficient number of radiosonde profiles are available for analysis during the winter for the results to be truly representative. To avoid any influence on the results from the tropopause, the lower limit of the data to be analyzed is set at 15 km altitude.

To identify gravity waves, the residual perturbations of the temperature, wind speed, and pressure profiles are needed. To remove the background atmosphere, a second-order polynomial is fitted to each individual profile and then removed [Vincent *et al.*, 1997]. The residual perturbation profile is representative of the gravity waves that the radiosonde has passed through on its ascent. The details of how the individual waves are extracted and their properties calculated are outlined in the next section.

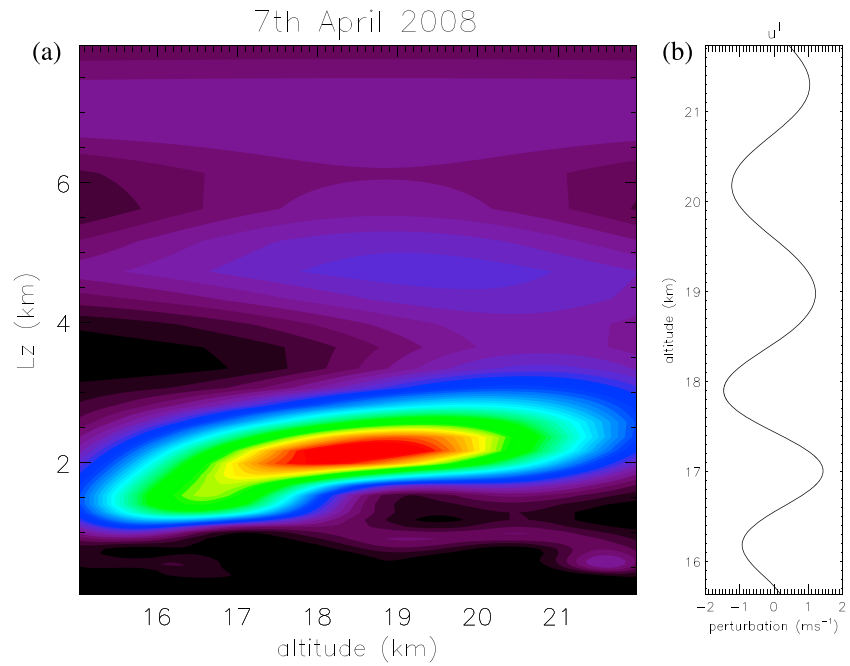


Figure 2. (a) Surface plot of the combined wavelet transform of radiosonde data from 7 April 2008. (b) Zonal wind perturbation reconstructed from main feature seen in Figure 2a.

2.1. Extraction of Individual Gravity Waves

The individual gravity waves are identified and extracted using the method outlined in *Zink and Vincent* [2001a]. A wavelet transform with a Morlet base [Torrence and Compo, 1998] is first applied to the meridional and zonal wind perturbation profiles. These wavelet transformed profiles are combined as in equation (1):

$$S_{u,v}(\lambda_z, z) = |W_u(\lambda_z, z)|^2 + |W_v(\lambda_z, z)|^2 \quad (1)$$

where S is the resulting surface value and W is the wavelet transform of the meridional (v) or zonal wind (u) perturbation profile in vertical wavelength (λ_z)-altitude (z) space.

Wave events are identified by local maxima in $S_{u,v}$; the boundaries of the wave event are set by locating where $S_{u,v}$ falls to one fourth of the local maximum value (or starts to rise again, whichever occurs first) [Zink and Vincent, 2001a]. The wind and temperature perturbation profiles are then created by applying reverse wavelet transforms [Torrence and Compo, 1998] to the wave event extracted from $S_{u,v}$. Figure 2 shows an example of $S_{u,v}$ and the resulting zonal wind perturbation profile for the main identified wave in Figure 2a. These perturbation profiles are then used to calculate the wave's characteristics.

3. Results

The techniques used to calculate the gravity wave parameters have typically been applied to whole profiles [Vincent and Alexander, 2000; Vincent et al., 1997; Yoshiki and Sato, 2000]. The presence of multiple waves in a profile may lead to incorrect results as the calculations used rely on the assumption of a single monochromatic wave being present [Zink and Vincent, 2001a]. In this study, the use of the wavelet technique will allow a more reliable representation of the gravity wavefield characteristics [Murphy et al., 2014; Zink and Vincent, 2001a, 2001b] as it identifies the individual waves. However, due to the nature of the Morlet wavelet (a 5 cycle sinusoidal wave in Gaussian envelope) used in the wavelet technique, there will be a bias toward those waves with a vertical wavelength of ≤ 2 km. Thus, gravity waves with longer vertical wavelengths will not be as clearly picked up by the technique [Murphy et al., 2014].

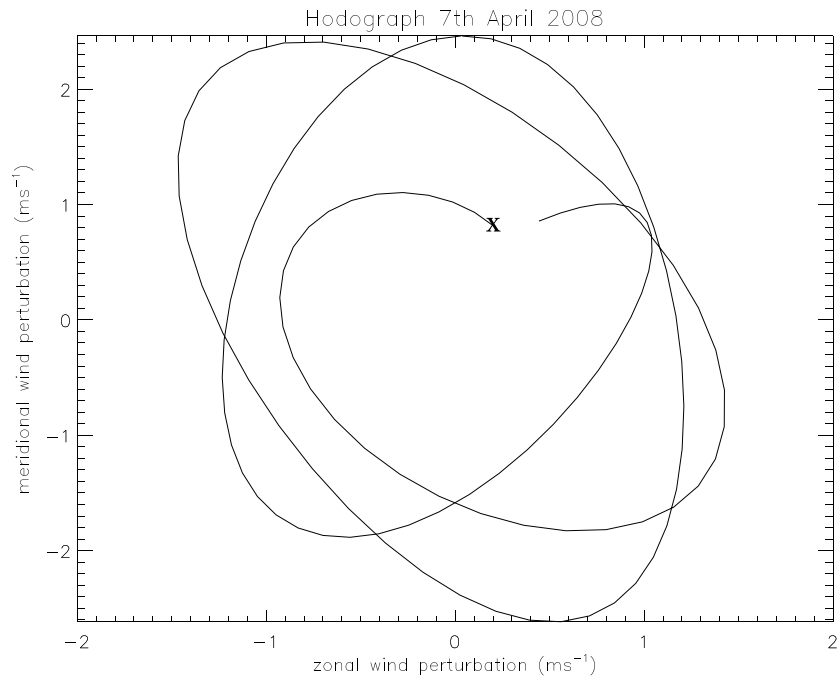


Figure 3. A hodograph plot using data from the same event shown in Figure 2. The cross marks the position of lowest altitude in the data.

In 10 years of Halley radiosonde data examined in this paper, 5883 waves have been successfully identified in the altitude range 15 km to 22 km. The results presented in this section are separated into upward and downward propagating wave climatologies to enable any differences in their characteristics to be examined and to determine how much energy density and momentum flux downward propagating waves are responsible for.

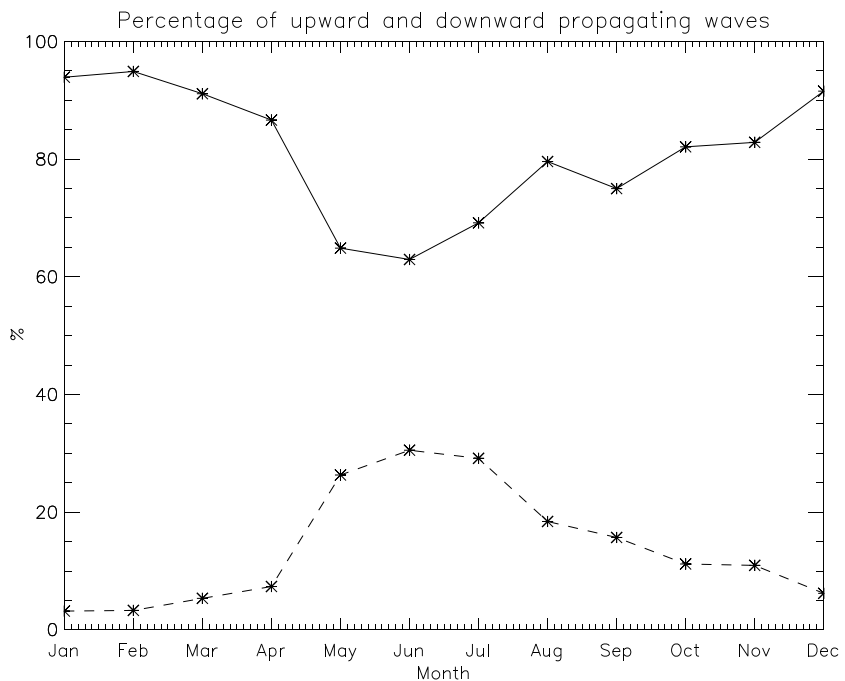


Figure 4. The monthly mean percentage of upward and downward propagating waves, between 15 km and 22 km altitude, determined using Halley radiosonde data from 2003 to 2013. Solid line is the percentage of upward propagating waves; dashed line is the percentage for downward propagating waves.

Table 1. The Monthly Mean Number of Upward and Downward Propagating Waves

	Jan	Feb	Mar	Apr	May	Jun	Jul	Aug	Sep	Oct	Nov	Dec
Upward	66	60	53	56	29	24	33	23	32	53	51	58
Downward	2	2	3	5	11	7	9	5	6	7	6	4

3.1. Direction of Propagation

The horizontal and vertical direction of propagation of a gravity wave can be determined using the relationship between the meridional and zonal wind perturbation profiles for the individual waves [Moffat-Griffin *et al.*, 2011; Vincent *et al.*, 1997]. The meridional and zonal wind perturbations for each wave are plotted against each other producing a hodograph (see Figure 3), and an average ellipse is fitted to the hodograph plot.

In the Southern Hemisphere a gravity wave propagating with energy upward will present a hodograph where the rotation of the ellipse (as altitude increases) is anticlockwise. A gravity wave with energy propagating downward will thus have a clockwise rotation [Hirota and Niki, 1985].

The hodograph method was applied to each of the extracted gravity waves. Figure 4 shows the 10 year, monthly average of the percentage of upward and downward propagating waves. It can be seen that there is an increase in the percentage of downward propagating waves in the wavefield during May to August up to 30%.

Table 1 shows the monthly mean number of upward and downward propagating waves for the data set. It can be seen that the percentage increase seen in Figure 4 is due to a combination of a reduction in the number of upward propagating waves and an increase in the number of downward propagating waves.

The horizontal direction of propagation is the same orientation as the major axis of the mean ellipse from the hodograph. However, this value has a 180° ambiguity. This ambiguity can be eliminated by applying a Hilbert transform to the wave’s temperature perturbation profile. It is then multiplied with the wind perturbation component parallel to the major axis of the ellipse before being averaged over height. This sign of this resulting value gives the direction of propagation [Hamilton, 1991; Vincent *et al.*, 1997].

Figure 5a shows the monthly horizontal direction of propagation for upward propagating waves in the form of a polar histogram. Figure 5b shows the same but for downward propagating waves. For both upward and downward propagating waves these results show that westward propagation dominates between March and November. During the summer months the wavefield does not exhibit a dominant direction.

3.2. Intrinsic Frequency and Wavelengths

The hodograph can also be used to calculate the intrinsic frequency, ω . The axial ratio (ratio of the wind components along the minor and major axes of the ellipse) is used to calculate the intrinsic frequency (equation (2)). A shear in the component of the wind transverse to the direction of propagation can alter the axial ratio; this is taken into account with the last term in equation (2) [Hines, 1989].

$$AR = \left| \frac{f}{\omega} - \frac{1}{N} \frac{dV_T}{dz} \right| \quad (2)$$

where N is the Brunt-Väisälä frequency, f the Coriolis frequency, and V_T the velocity component transverse to the direction of propagation.

For ease of comparisons with other studies the ω/f ratio for upward and downward propagating waves are presented as histograms in Figure 6.

Figure 6 shows that the upward propagating wave distribution is dominated by waves, where $\omega \sim f$, with higher-frequency waves being present but not as numerous. Downward propagating waves do not show such a clear distribution with wave frequencies, with higher frequency waves being about half as prevalent as lower frequency ones.

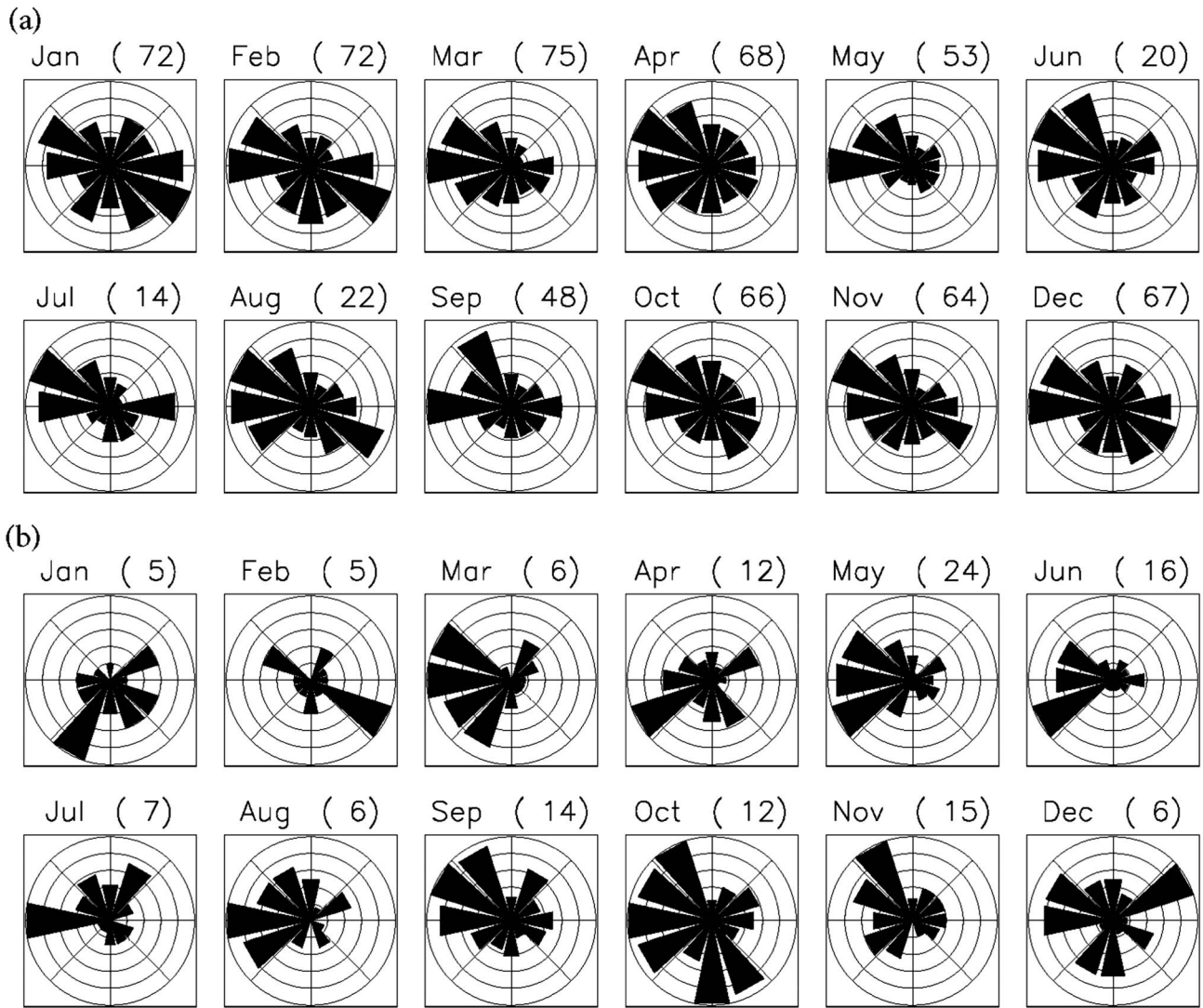


Figure 5. (a) Monthly histograms of horizontal propagation direction of upward propagating gravity waves. The outer ring on each histogram (number of waves in that direction bin) is the value in brackets next to the month title; each bin is 45°. Northward is at the top of the plots, with eastward being to the right. (b) As in Figure 5a but for downward propagating waves.

The vertical wavelength (λ_z) is extracted from the wavelet analysis technique where it is taken at the local maximum of the wave event that is identified. Using the vertical wave number, $m (=2\pi/\lambda_z)$, and the intrinsic frequency, ω , the horizontal wave number ($k_h = 2\pi/\lambda_h$) can be calculated using the dispersion relationship as shown in equation (3) [Fritts and Alexander, 2003].

$$k_h^2 = \frac{m^2(\omega^2 - f^2)}{N^2} \quad (3)$$

Figures 7 and 8 show histograms of the vertical and horizontal wavelengths, respectively. In Figure 7 we see a peak in the upward propagating waves that is around 1 km and below. This is expected due to the bias toward waves with a vertical wavelength of ≤ 2 km that is a result of the wavelet analysis technique used. For this study an altitude range of 7 km is used; thus, vertical wavelengths greater than 3.5 km would not be able to be detected. The downward propagating waves show a flatter distribution, with a peak around 1 km but also a smaller peak around 3.5 km.

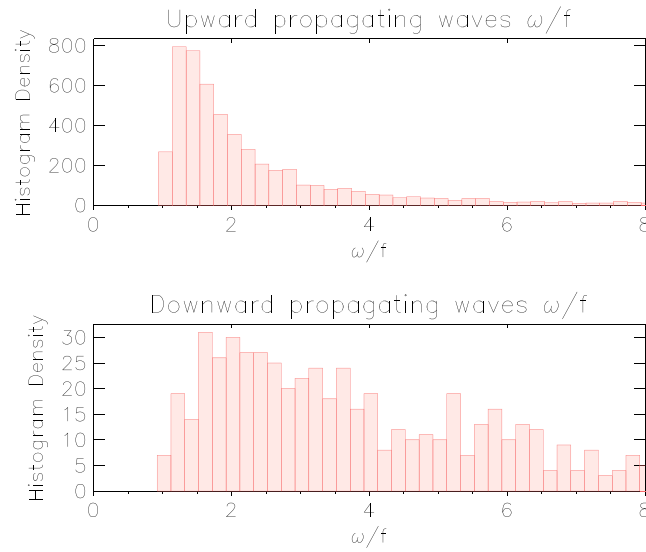


Figure 6. Histogram showing the ω/f ratio for (top) upward and (bottom) downward propagating waves.

$$E_k = \frac{1}{2} (\overline{u^2} + \overline{v^2}) \tag{4a}$$

$$E_p = \frac{1}{2} \frac{g^2}{N^2} \overline{\tilde{T}^2} \tag{4b}$$

where \tilde{T}^2 is the temperature perturbation divided by the background temperature. The overbar signifies averaging over height.

Figure 9 shows monthly average variations for E_k and E_p for both upward and downward propagating waves. For the upward propagating waves a small peak in E_k is observed in autumn with a much larger peak in spring. For E_p a small peak is seen in springtime. For downward propagating waves, E_k peaks during the winter months, coinciding with the increase in downward propagating waves seen in Figure 4. The E_p variation follows that of the upward propagating waves closely, with a small peak in springtime.

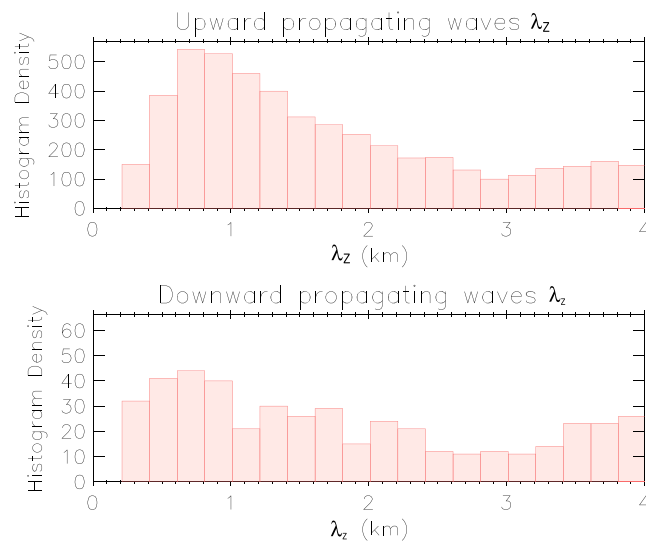


Figure 7. Same figure style as Figure 6 but for vertical wavelength (km).

Figure 8 shows a similar shape distribution for both upward and downward propagating waves. The dominant horizontal wavelengths for upward propagating waves are between 50 km and 150 km; for downward propagating waves the peak is between 25 km and 100 km.

3.3. Energy Density and Pseudomomentum Fluxes

The kinetic and potential energy density (equations (4a) and (4b), respectively) are calculated using the wind and temperature perturbations extracted from the wavelet transform.

The momentum flux of gravity waves can be calculated using the perturbation of vertical wind velocity multiplied by the perturbation of horizontal wind; however, the vertical wind velocity is not recorded as part of these radiosonde data, so a pseudomomentum flux calculation is used instead. Pseudomomentum flux (hereafter referred to as pMF) is calculated using the gravity wave polarization equations between the wind and temperature perturbations [Zink and Vincent, 2001a]. The upward flux of zonal and meridional momentum fluxes are calculated using equations (5a) and (5b), respectively.

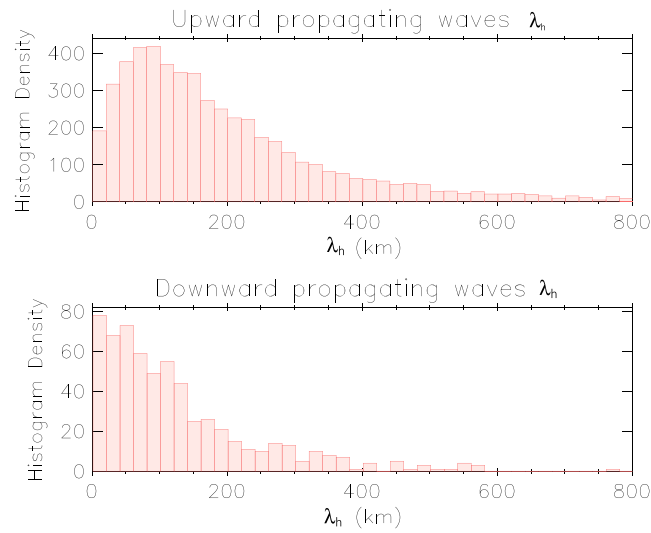


Figure 8. Same figure style as Figure 6 but for horizontal wavelength (km).

$$\overline{u'w'} = -\frac{\omega g}{N^2} \overline{u' \tilde{T}'_{+90}} \delta_- \quad (5a)$$

$$\overline{v'w'} = -\frac{\omega g}{N^2} \overline{v' \tilde{T}'_{+90}} \delta_- \quad (5b)$$

where \tilde{T}'_{+90} is the Hilbert transform of \hat{T}'^2 and $\delta_- = (1 - f^2/\omega^2)$.

Figure 10 shows the monthly averaged zonal and meridional pMF. The upward propagating wave zonal pMF shows larger values in the spring and autumn, following the trend seen in Figure 9. Both the upward and downward propagating wave fluxes are of the same sign and magnitude in the zonal direction.

However, the upward and down-

ward propagating meridional pMF, although of similar magnitudes, have the opposite sign for nearly half the year.

4. Discussion

4.1. Wave Characteristics

The maximum value of downward propagating waves is around 30%; this is lower than seen at other Antarctic sites (Moffat-Griffin et al., 2011, 2013; Murphy et al., 2014), where the percentage of downward propagating waves can exceed that of upward propagating waves.

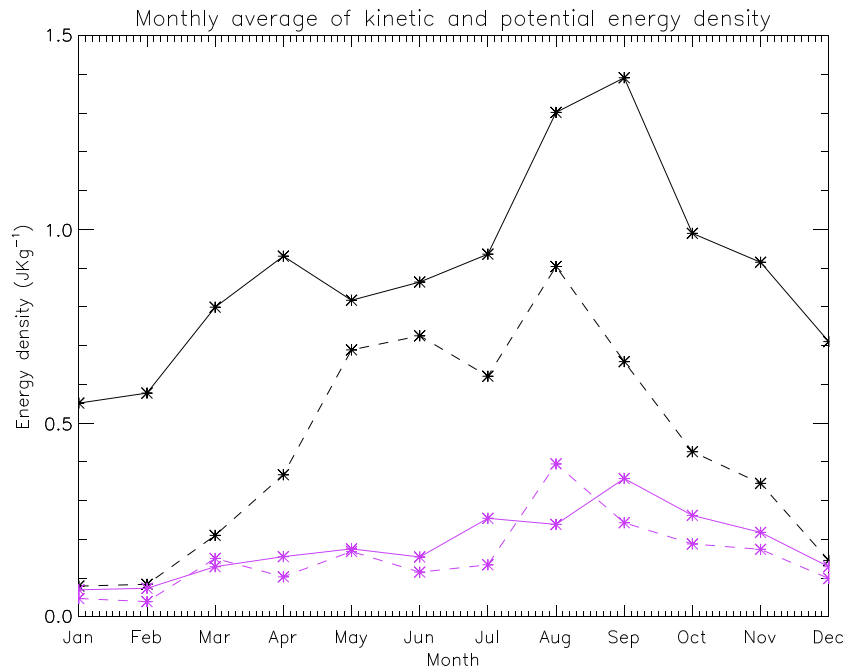


Figure 9. The monthly average kinetic (black) and potential (purple) energy densities for upward (solid line) and downward (dashed line) propagating waves.

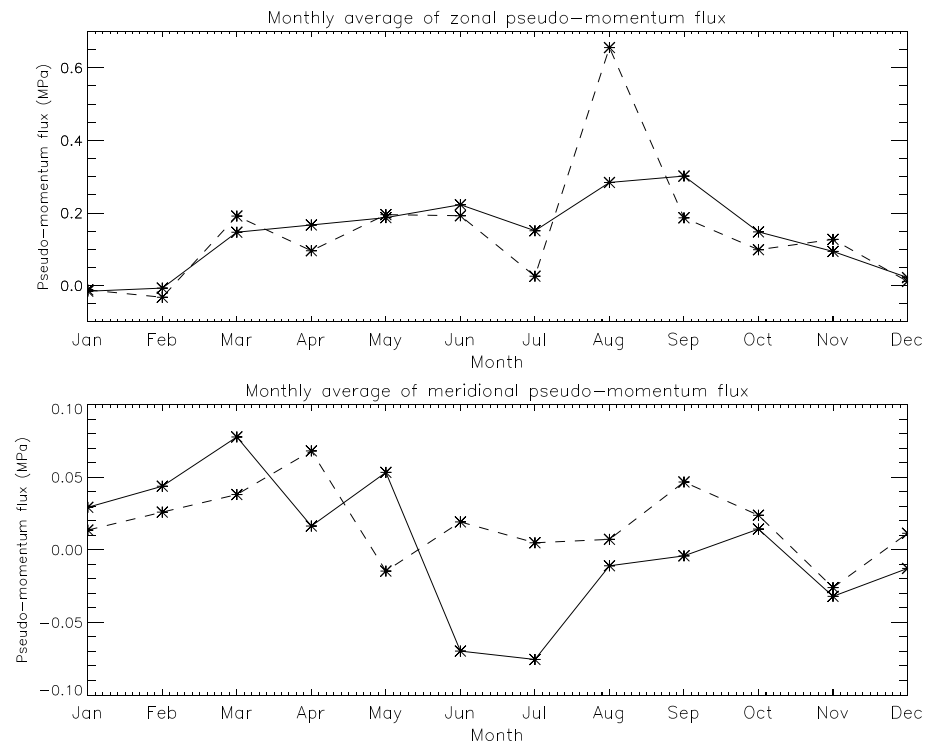


Figure 10. The monthly average (top) zonal and (bottom) meridional pseudomomentum flux for upward (solid line) and downward (dashed line) propagating waves.

The upward and downward propagating gravity wavefields in the lower stratosphere above Halley exhibit similar horizontal propagation directions: westward in the winter and no dominant direction in the summer. This is consistent with wind filtering by the strong eastward winds in the winter stratosphere. The eastward winds in summer are weaker, resulting in less waves being filtered out. They also exhibit a similar distribution in horizontal wavelengths.

The two characteristics where there is most difference between the two wavefields are the vertical wavelength and intrinsic frequency: There is a clearly defined peak in the distributions for upward propagating waves compared to the distributions for downward propagating waves. This shows that there are higher-frequency waves present in the downward propagating part of the wavefield.

A radiosonde study (which uses the same wavelet analysis technique as this paper) using radiosonde data from Davis, Antarctica ($68^{\circ}34'S$ $77^{\circ}58'E$), has shown near-equal numbers of upward and downward propagating waves in winter in the 15 km to 30 km altitude range. They also present histogram distribution shapes for intrinsic frequency and vertical and horizontal wavelengths that are very similar for both upward and downward propagating waves [see *Murphy et al.*, 2014, Figure 5].

A different radiosonde study (that uses the whole profile technique) on data from Syowa, Antarctica ($69^{\circ}S$ $39^{\circ}35'E$), shows downward propagating waves making up 43% of the wavefield in winter over an altitude range of 15–25 km. Their downward propagating histograms show a wider range of frequencies and vertical wavelengths which is comparable to Halley [*Yoshiki et al.*, 2004, Figures 6–8].

The wave characteristics seen at Halley are comparable to those observed over a similar altitude range at Syowa, although the percentage of the downward propagating waves is higher. The differences between the Halley and Davis results are most likely due to the larger height range used in the Davis study so more downward propagating waves are captured by their analysis technique.

The dominant source of downward propagating waves is thought to be the polar vortex, a strong circumpolar wind region that occurs in the winter polar stratosphere during the winter months. Work has shown that the instabilities associated with the stratospheric polar vortex can generate both upward and downward

Table 2. The Monthly Averaged Kinetic and Potential Energy Densities in the Lower Stratosphere Observed Using Radiosonde Data From Other Antarctic and Subantarctic Sites

Station	E_k (J kg ⁻¹)	E_p (J kg ⁻¹)	Altitude Range (km)	Analysis Method	Reference
Halley (75°S, 26°W)	0.6–1.9	0.04–0.2	15–22	Wavelet method, arithmetic mean	This study
Rothera (67°S, 68°W)	0.2–0.6	0.2–0.6	15–22	Whole profile, lognormal mean	<i>Moffat-Griffin et al.</i> [2011]
Syowa (69°S, 39°E)	0.1–0.8	0.2–0.5	15–20	Whole profile, arithmetic mean	<i>Yoshiki and Sato</i> [2000]
South Pole (90°S)	0.5–6	0.5–1.5	15–25	Whole profile	<i>Pfenninger et al.</i> [1999]
Davis (68°S, 77°E)	0.33–0.4	0.1–0.13	15–22	Wavelet analysis, lognormal mean	<i>Murphy et al.</i> [2014]
Macquarie Island (55°S, 159°E)	1.1–4.5	0.8–2.2	12–25	Whole profile	<i>Vincent et al.</i> [1997]
Falkland Islands (51°S, 58°W)	0.5–1	0.5	15–22	Whole profile, lognormal mean	<i>Moffat-Griffin et al.</i> [2013]

propagating gravity waves [*Sato and Yoshiki*, 2008; *Whiteway et al.*, 1997; *Yoshiki and Sato*, 2000; *Yoshiki et al.*, 2004]. *Murphy et al.* [2014] have examined the residuals of the nonlinear balance equation to identify regions where instabilities occur. Their work shows that during the winter months, at Halley's position (75°35'S, 26°39'W), there is a weak region of instability. This is likely the source of the increase in downward propagating waves that we see in our study. Both Syowa and Davis are located within the higher region of instability (as they are at a lower latitude ~69°S). The altitude range of this instability is such that it extends way above the upper altitude limit for this study. These two factors combined explain why we see fewer downward propagating waves at Halley compared to these other sites.

4.2. Energy Density of the Wavefield

Both kinetic and potential energy density associated with upward propagating waves increase in springtime. This is consistent with other radiosonde studies at other Antarctic stations of the total kinetic and potential energy density (combined upward and downward propagating waves) [*Innis et al.*, 2004; *Moffat-Griffin et al.*, 2011; *Murphy et al.*, 2014; *Yoshiki and Sato*, 2000]. The downward propagating wave kinetic energy density shows a large increase in the wintertime (increasing from near 0 to 0.75 J kg⁻¹); this coincides directly with their increase in numbers (see Table 1).

Comparing the energy density magnitudes of different Antarctic radiosonde studies is not straightforward as different methods and altitude ranges have been used to calculate them, as explained in *Murphy et al.* [2014]. This study is the first to present results where the upward and downward propagating wave energy densities have been separated. In order to compare these results with other studies, they are added together. Table 2 shows the values observed at other Antarctic sites. Where a study uses a lognormal average to calculate the energy density, it can be assumed that these values are a factor of 2 smaller than when the arithmetic mean is used [*Murphy et al.*, 2014].

As each study uses a slightly different technique and altitude range, this is not a direct comparison. For example, those studies which used a wavelet method will have lower values for energy density compared to other methods as the wavelet will not have captured all the waves present. Taking this into account, the values seen at Halley are of a similar range to those seen at most other stations.

The differences between the seasonal variations of E_k and E_p for upward and downward propagating waves can be explained when the frequency of the different wavefields is examined. It has been shown that E_k is sensitive to low-frequency gravity waves and that E_p is sensitive to both high- and low-frequency waves [*Geller and Gong*, 2010]. This study has shown that the downward propagating wavefield is made up of a wider range of frequencies than the upward propagating wavefield (see Figure 6). With this in mind and examining Figure 9, it would suggest that although the downward propagating wavefield contains a higher proportion of higher-frequency waves than the upward propagating wavefield these do not contribute greatly to the observed E_p as the purple dashed and solid lines in Figure 9 are of similar magnitude.

However, the kinetic energy density during June is similar for both upward and downward propagating waves even though the latter make up only 30% of the wavefield.

4.3. Pseudomomentum Flux of the Wavefield

The monthly average zonal pMF of both upward and downward propagating waves is generally larger than the meridional pMF (a maximum value of 0.3 mPa compared to 0.08 mPa). For upward propagating waves

the zonal pMF increases steadily throughout the winter until it peaks in September (coinciding with the peak in E_k). For downward propagating waves there is more variability but the flux is larger during the winter.

Murphy *et al.* [2014] separated out their pseudomomentum fluxes into seasonal upward and downward propagating components. There is good agreement between the Davis and Halley results: positive values of a similar magnitude of zonal and meridional pMF for upward propagating waves in both winter and summer. For the downward propagating waves the same level of agreement in sign and magnitude is seen. The percentage of downward propagating waves seen over Halley compared to Davis is slightly lower. A potential explanation for this could be that a larger altitude range is used in the Davis study; thus, they are able to observe more waves.

5. Conclusions

The lower stratosphere gravity wavefield above Halley is dominated year-round by upward propagating low-frequency gravity waves. During the winter months there is an increase in the percentage of downward propagating waves (although lower than what is seen at other Antarctic sites). Although the downward propagating wavefield contains a spread of low and high intrinsic frequency, waves it has been shown that these higher-frequency waves do not contribute strongly to the observed energy density of the downward propagating wavefield.

During midwinter it has been shown that the downward propagating waves in the lower stratosphere above Halley contribute as much to the total energy density and pMF of the wavefield as the upward propagating waves. This is despite the downward propagating waves making up only 30% of the wavefield.

This study has shown that low-frequency gravity waves are prevalent in the lower stratosphere above Halley and that the downward propagating waves are especially important during the winter months where they contribute as much as the upward propagating waves in terms of energy and momentum.

Acknowledgments

The field staff at Halley station are acknowledged for their work in ensuring a near-daily radiosonde launch occurs even in the depths of the Antarctic winter. The raw data used in this study can be found at the Centre for Environmental Data Analysis (CEDA): <http://catalogue.ceda.ac.uk/uuid/2e829bcad8ac653ceb6eef4c6107773f>.

References

- Alexander, M. J. (1998), Interpretations of observed climatological patterns in stratospheric gravity wave variance, *J. Geophys. Res.*, *103*(D8), 8627–8640, doi:10.1029/97JD03325.
- Alexander, M. J., S. D. Eckermann, D. Broutman, and J. Ma (2009), Momentum flux estimates for South Georgia Island mountain waves in the stratosphere observed via satellite, *Geophys. Res. Lett.*, *36*, L12816, doi:10.1029/2009GL038587.
- Alexander, M. J., et al. (2010), Recent developments in gravity wave effects in climate models, and the global distribution of gravity wave momentum flux from observations and models, *Q. J. R. Meteorol. Soc.*, *136*(650), 1103–1124.
- Espy, P. J., R. E. Hibbins, G. R. Swenson, J. Tang, M. J. Taylor, D. M. Riggin, and D. C. Fritts (2006), Regional variations of mesospheric gravity-wave momentum flux over Antarctica, *Ann. Geophys.*, *24*, 81–88.
- Fritts, D. C., and M. J. Alexander (2003), Gravity wave dynamics and effects in the middle atmosphere, *Rev. Geophys.*, *41*(1), 1003, doi:10.1029/2001RG000106.
- García, R. R., A. K. Smith, D. E. Kinnison, Á. de la Cámara, and D. J. Murphy (2017), Modification of the gravity wave parameterization in the whole atmosphere community climate model: Motivation and results, *J. Atmos. Sci.*, *74*(1), 275–291.
- Gardner, C. S., and N. F. Gardner (1993), Measurement distortion in aircraft, space shuttle, and balloon observations of atmospheric density and temperature perturbation spectra, *J. Geophys. Res.*, *98*(D1), 1023–1033, doi:10.1029/92JD02025.
- Geller, M. A., and J. Gong (2010), Gravity wave kinetic, potential, and vertical fluctuation energies as indicators of different frequency gravity waves, *J. Geophys. Res.*, *115*, D11111, doi:10.1029/2009JD012266.
- Gong, J., D. L. Wu, and S. D. Eckermann (2012), Gravity wave variances and propagation derived from AIRS radiances, *Atmos. Chem. Phys.*, *12*(4), 1701–1720.
- Guest, F. M., M. J. Reeder, C. J. Marks, and D. J. Karoly (2000), Inertia-gravity waves observed in the lower stratosphere over Macquarie Island, *J. Atmos. Sci.*, *57*(5), 737–752.
- Hamilton, K. (1991), Climatological statistics of stratospheric inertia-gravity waves deduced from historical rocketsonde wind and temperature data, *J. Geophys. Res.*, *96*, 20,831–20,839, doi:10.1029/91JD02188.
- Hertzog, A., G. Boccaro, R. A. Vincent, F. Vial, and P. Cocquerez (2008), Estimation of gravity wave momentum flux and phase speeds from quasi-Lagrangian stratospheric balloon flights. Part II: Results from the Vorcore Campaign in Antarctica, *J. Atmos. Sci.*, *65*(10), 3056–3070.
- Hertzog, A., et al. (2007), Stratéole/Vorcore—Long-duration, superpressure balloons to study the Antarctic lower stratosphere during the 2005 winter, *J. Atmos. Ocean. Technol.*, *24*(12), 2048–2061.
- Hindley, N. P., C. J. Wright, N. D. Smith, and N. J. Mitchell (2015), The southern stratospheric gravity wave hot spot: Individual waves and their momentum fluxes measured by COSMIC GPS-RO, *Atmos. Chem. Phys.*, *15*(14), 7797–7818.
- Hines, C. Q. (1989), Tropopausal mountain waves over Arecibo: A case study, *J. Atmos. Sci.*, *46*(4), 476–488.
- Hirota, I., and T. Niki (1985), A statistical study of inertia-gravity waves in the middle atmosphere, *J. Meteorol. Soc. Jpn.*, *63*, 1055–1066.
- Innis, J. L., A. R. Klekociuk, and R. A. Vincent (2004), Interstation correlation of high-latitude lower-stratosphere gravity wave activity: Evidence for planetary wave modulation of gravity waves over Antarctica, *J. Geophys. Res.*, *109*, D17106, doi:10.1029/2004JD004961.
- McLandsress, C., and J. F. Scinocca (2005), The GCM response to current parameterizations of nonorographic gravity wave drag, *J. Atmos. Sci.*, *62*, 2394–2413.
- Moffat-Griffin, T., R. E. Hibbins, M. J. Jarvis, and S. R. Colwell (2011), Seasonal variations of gravity wave activity in the lower stratosphere over an Antarctic Peninsula station, *J. Geophys. Res.*, *116*, D14111, doi:10.1029/2010JD015349.

- Moffat-Griffin, T., M. J. Jarvis, S. R. Colwell, A. J. Kavanagh, G. L. Manney, and W. H. Daffer (2013), Seasonal variations in lower stratospheric gravity wave energy above the Falkland Islands, *J. Geophys. Res. Atmos.*, *118*, 10,861–10,869, doi:10.1002/jgrd.50859.
- Moffat-Griffin, T., M. J. Taylor, T. Nakamura, D. J. Murphy, and J. V. Bageston (2016), ANtarctic Gravity Wave Instrument Network (ANGWIN) webpage: <https://www.bas.ac.uk/project/angwin/>, edited.
- Murphy, D. J., S. P. Alexander, A. R. Klekociuk, P. T. Love, and R. A. Vincent (2014), Radiosonde observations of gravity waves in the lower stratosphere over Davis, Antarctica, *J. Geophys. Res. Atmos.*, *119*(21), 11,973–11,996, doi:10.1002/2014JD022448.
- Pfenninger, M., A. Z. Liu, G. C. Papen, and C. S. Gardner (1999), Gravity wave characteristics in the lower atmosphere at south pole, *J. Geophys. Res.*, *104*(D6), 5963–5984.
- Sato, K., and M. Yoshiki (2008), Gravity wave generation around the polar vortex in the stratosphere revealed by 3-hourly radiosonde observations at Syowa Station, *J. Atmos. Sci.*, *65*(12), 3719–3735.
- Smout, R., J. Nash, T. Hewison, and M. Smees (2005), Results of the RS92 acceptance test performed by the Met Office (UK), Rep., WMO.
- Steinbrecht, W., H. Claude, F. Schönenborn, U. Leiterer, H. Dier, and E. Lanzinger (2008), Pressure and temperature differences between Vaisala RS80 and RS92 radiosonde systems, *J. Atmos. Ocean. Technol.*, *25*(6), 909–927.
- Torrence, C., and G. P. Compo (1998), A practical guide to wavelet analysis, *Bull. Am. Meteorol. Soc.*, *79*(1), 61–78.
- Vaisala (2013), RS92-SGP datasheet, edited.
- Vincent, R., S. J. Allen, and E. Eckermann (1997), Gravity-wave parameters in the lower stratosphere, in *Gravity Wave Processes: Their Parameterization in Global Climate Models*, edited by K. Hamilton, pp. 7–25, Springer, New York.
- Vincent, R. A., and M. J. Alexander (2000), Gravity waves in the tropical lower stratosphere: An observational study of seasonal and interannual variability, *J. Geophys. Res.*, *105*(D14), 17,971–17,982, doi:10.1029/2000JD900196.
- Wang, L., and M. J. Alexander (2010), Global estimates of gravity wave parameters from GPS radio occultation temperature data, *J. Geophys. Res.*, *115*, D21122, doi:10.1029/2010JD013860.
- Whiteway, J. A., T. J. Duck, D. P. Donovan, J. C. Bird, S. R. Pal, and A. I. Carswell (1997), Measurements of gravity wave activity within and around the Arctic stratospheric vortex, *Geophys. Res. Lett.*, *24*(11), 1387–1390, doi:10.1029/97GL01322.
- Wright, C. J., N. P. Hindley, A. C. Moss, and N. J. Mitchell (2016), Multi-instrument gravity-wave measurements over Tierra del Fuego and the Drake Passage—Part 1: Potential energies and vertical wavelenghts from AIRS, COSMIC, HIRDLS, MLS-Aura, SAAMER, SABER and radiosondes, *Atmos. Meas. Tech.*, *9*(3), 877–908.
- Wu, D. L., and J. H. Jiang (2002), MLS observations of atmospheric gravity waves over Antarctica, *J. Geophys. Res.*, *107*(D24), 4773, doi:10.1029/2002JD002390
- Yamashita, C., X. Chu, H.-L. Liu, P. J. Espy, G. J. Nott, and W. Huang (2009), Stratospheric gravity wave characteristics and seasonal variations observed by lidar at the South Pole and Rothera, Antarctica, *J. Geophys. Res.*, *114*, D12101, doi:10.1029/2008JD011472.
- Yoshiki, M., and K. Sato (2000), A statistical study of gravity waves in the polar regions based on operational radiosonde data, *J. Geophys. Res.*, *105*(D14), 17,995–18,011, doi:10.1029/2000JD900204.
- Yoshiki, M., N. Kizu, and K. Sato (2004), Energy enhancements of gravity waves in the Antarctic lower stratosphere associated with variations in the polar vortex and tropospheric disturbances, *J. Geophys. Res.*, *109*, D23104, doi:10.1029/2004JD004870.
- Zink, F., and R. A. Vincent (2001a), Wavelet analysis of stratospheric gravity wave packets over Macquarie Island: 1. Wave parameters, *J. Geophys. Res.*, *106*, 10,275–10,288, doi:10.1029/2000JD900847.
- Zink, F., and R. A. Vincent (2001b), Wavelet analysis of stratospheric gravity wave packets over Macquarie Island: 2. Intermittency and mean-flow accelerations, *J. Geophys. Res.*, *106*(D10), 10,289–10,297, doi:10.1029/2000JD900846.